






©2025 IEEE. Personal use of this material is permitted. Permission from IEEE must be obtained for all other uses, in any current or future media, including reprinting/republishing this material for advertising or promotional purposes, creating new collective works, for resale or redistribution to servers or lists, or reuse of any copyrighted component of this work in other works.

Article Information

Article Type:	research
Journal Title:	IEEE Transactions on Microwave Theory and Techniques
Publisher:	IEEE
DOI Number:	10.1109/TMTT.2025.3640952
Volume Number:	0
Issue Number:	
First Page:	1
Last Page:	10
Copyright:	0018-9480 © 2025 IEEE. All rights reserved, including rights for text and data mining, and training of artificial intelligence and similar technologies. Personal use is permitted, but republication/redistribution requires IEEE permission. See https://www.ieee.org/publications/rights/index.html for more information.
Revised1 Date:	10-11-2025
Accepted Date:	29-11-2025
↑	

Novel Regular Hexagonal Six-Port Hybrid Couplers for Multibeam AQ1 Applications

 **Zhiwei Yin**, Graduate Student Member¹,  **He Zhu**, Senior Member²,  **Xiaojing Lv**, Member¹,  **Jiexin Lai**, Member¹ and  **Yang Yang**, Senior Member yang.yang.au@ieee.org¹

¹School of Electrical and Data Engineering, University of Technology Sydney, Sydney, NSW 2007, Australia

²Manufacturing, Commonwealth Scientific and Industrial Research Organisation (CSIRO), West Lindfield, NSW 2070, Australia

(Corresponding author: Yang Yang.)

Abstract

This article proposes a novel approach to implementing the 3-beam Nolen matrix (NM) using a compact planar six-port regular hexagonal coupler for multibeam applications. Compared to conventional NM designs, this design could significantly reduce the size of the matrix by using a regular hexagonal coupler. The six-port hybrid coupler is composed of two hexagons and a series of transmission lines connecting them. The power at each output port can be controlled by the impedance of the transmission lines. To verify this, two six-port couplers with the power division ratios of 1:1:1 and 1:2:1 are designed. The transmission coefficient of the first design is 5 ± 0.38 dB. The return loss exceeds 20 dB, while the amplitude and phase fluctuations are within 0.9 dB and 14°, respectively, across 2.28–2.61 GHz. In addition, the return loss and isolation of the second design are better than 13.6 dB, while isolation is greater than 15.8 dB across 2.3–2.6 GHz. The size of these two six-port regular hexagonal couplers is both $2.59 \times 0.37\lambda_0^2$, where $0.37\lambda_0$ represents the side length of this hexagonal shape, respectively. Furthermore, two prototypes are introduced to demonstrate the simplicity and effectiveness of the proposed approach in implementing both equal and unequal power division beamforming networks, while maintaining excellent RF performance in a

compact design.

Graphical Abstract

Keywords

Beam-forming network (BFN), multibeam applications, Nolen matrix (NM), regular hexagonal coupler, six-port, unequal power division

Note: The full funding statement, if included, is available on the proof PDF, which can be viewed by clicking on PDF in the top toolbar.

Funding

University of Technology Sydney (UTS) Australian Research Council (ARC) Future Fellow Near Miss Support

Nano Dimension Ph.D. Scholarship

ARC Linkage Projects LP210300004, LP230200030

ARC Linkage Infrastructure LE220100035

I. Introduction

BEAM-FORMING networks (BFNs) play a crucial role in modern wireless communication systems, particularly in multiple-input multiple-output (MIMO) and multibeam antenna applications [1], [2]. Among various BFN architectures, the Nolen matrix (NM) has emerged as a significant solution, offering unique advantages in terms of flexibility and performance [3], [4]. The NM architecture traditionally consists of directional couplers and phase shifters arranged in a specific topology that enables the synthesis of desired beam patterns [5]. Unlike its counterparts, such as the Butler matrix (BM) [6], [7], [8], [9], [10], [11], [12] or Blass matrix [13], [14], [15], the NM offers greater flexibility in terms of the number of input and output ports, making it particularly suitable for asymmetric beam-forming applications [16]. This flexibility allows for customized power distribution and phase relationships between different ports, enabling sophisticated beam-steering capabilities and pattern

synthesis [17]. However, NM implementations often face challenges related to circuit complexity, size, and performance fluctuation due to the cascaded arrangement of multiple couplers and phase shifters.

To simplify the NM architecture while maintaining or enhancing its beam-forming capabilities, efforts have been made in previous works. For instance, vertically installed planar couplers with 180° phase difference are presented in [18] and [19] to replace traditional planar structures. This vertical mounting approach effectively reduces the footprint of the NM, enabling more compact designs. Designs will be bulky as multiple layers are adopted. In [20], a new type of couplers integrates the functionalities of both couplers and phase shifters into a single component, which offers a significant advantage over conventional designs. This combination of coupling values and phase differences enables a significant reduction in the number of required phase shifters, resulting in a compact overall size of $0.95\lambda_0 \times 0.5\lambda_0$. Building upon this approach, researchers in [21] extended the concept to develop two distinct 3×3 BFNs, providing five-beam and six-beam options, respectively. A further advancement in miniaturization is presented in [22], where researchers achieved even more size reduction through the complete integration of phase shifters within hybrid couplers. Extending to the second plane, a 2-D one-body multibeam NM was presented in [23]. These advanced miniaturization approaches in NM designs mark a significant leap from the contribution of single key components to the integration of two or more components into one hybrid coupler. Although these designs achieve integration and size reduction, they suffer from high design complexity and implementation challenges in nonplanar structures, which limit their scalability and practicality.

To further address the size issue, another approach is to replace a three-way NM with a six-port hybrid coupler by integrating all four-port couplers, hybrid couplers, and phase shifters. A dual-layer three-way directional coupler is implemented as a 3×3 BFN to provide orthogonal three-beam switching capability [24]. Due to the necessity of jump lines, it cannot be realized in a planar structure. In addition, the three-way couplers are essential building blocks for extending larger BM, serving as key components for power division and phase control in expanded beamforming networks, such as 5×6 , 6×6 , and 9×9 BM [2], [25], [26], [27], [28], [29]. Expanding on this idea, researchers in [26] proposed a 6×6 BFN capable of generating six beams based on the three-way

directional coupler. Similarly, [27] describes the topology of a modified 5×6 BFN that uses a three-way directional coupler to generate five beams. While this design achieves an overall size of $1.2\lambda_0 \times 1.7\lambda_0$, its nonplanar structure remains a significant drawback. In addition, several studies have explored the use of substrate-integrated waveguide (SIW) technology to implement three-way directional couplers [2], [28]. These SIW-based couplers are designed for different application scenarios compared to microstrip line structures. Similarly, the 6×6 ridge gap waveguide (RGW) BFN is realized by aluminum alloy 3F printing technology [29]. However, their larger dimensions make them less suitable for multiple utilizations as core components in complex BFNs, particularly in space-constrained applications.

In this article, a novel compact planar six-port hybrid coupler is proposed to replace the 3×3 NM with the same magnitude and phase features. Compared with existing three-way coupler designs in the literature, this work has unique advantages of compact size, low loss, and simple configuration. This work represents a substantial extension of the previous conference paper [11]. Our conference work employed additive manufacturing to realize a 3-D BM for size reduction. This work advances that concept by introducing a compact six-port hexagonal coupler to replace the conventional 3×3 NM, achieving miniaturization with a uniplanar PCB implementation. The main contributions of this work can be summarized as follows.

1. A compact planar six-port hexagonal coupler is proposed to replace the conventional 3×3 NM with over 70% size reduction.
2. A systematic design theory and explicit formula set are developed, providing clear design procedures that enhance applicability and reproducibility.
3. Two prototypes with equal and unequal power ratios are designed and validated, demonstrating flexibility for varied beamforming needs.
4. The proposed simple configuration provides huge potential for integration into both large-scale and compact beamforming systems.

The rest of this article is organized into four sections. [Section II](#) outlines the working principle and topology development of the proposed planar coupler. [Section III](#) details the design of two key components: the equal and unequal power ratio six-port coupler. [Section IV](#) covers the fabrication,

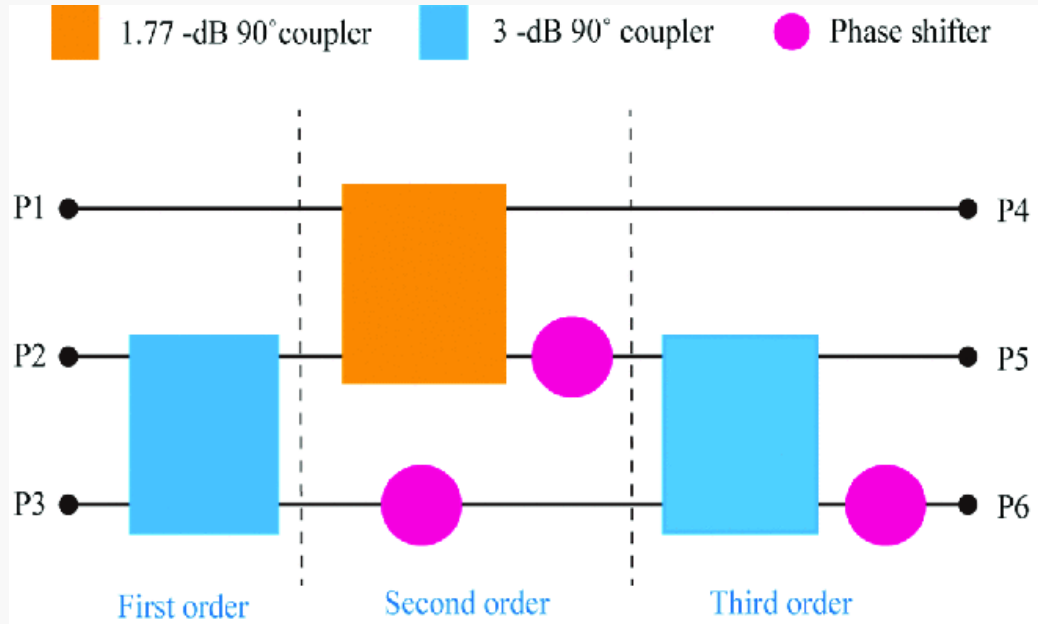
measurement, and discussion of the planar six-port coupler. [Section V](#) summarizes the contributions of the work and discusses future perspectives.

II. Proposed Topology of Six-Port Coupler and Analysis

A convenient topology of the uniplanar 3×3 NM is shown in [Fig. 1\(a\)](#) [23], which is a third-order structure, including a 1.77-dB coupler, a pair of 3-dB couplers, and three phase shifters. Each coupler typically generates a quadrature phase difference. When the input ports (Ports 1–3) are individually excited, the signal splits equally among Ports 4–6. The three phase shifters introduce appropriate phase shifts of 180° , 90° , and 90° . Considering the initial phase of the first column element normalized to the reference phase, the 3×3 BFN transmission can be expressed, using the elementary determinant transformation, as

$$T_{\text{NM}} = \begin{bmatrix} 1 & 1 & 1 \\ 1 & e^{-j\frac{\pi}{2}} & e^{j\frac{\pi}{2}} \\ 1 & e^{j\frac{\pi}{2}} & e^{-j\frac{\pi}{2}} \end{bmatrix}. \quad (1)$$

Fig. 1. Topology of (a) traditional uniplanar 3×3 NM topology. (b) Proposed BFN using a six-port coupler.



Uniplanar 3×3 Nolen matrix

(a)



Proposed 3×3 BFN

(b)

The phase difference between any element in each row and the neighboring subsequent element is 0° , 120° , and -120° , respectively. To reduce the effort in components and improve the integration of

BFN, couplers and related phase shifters are integrated into hybrid couplers. Further up, the proposed topology of BFN is presented to simplify the constitution of the 3×3 NM. As illustrated in Fig. 1(b), the proposed circuit only includes one six-port component, thereby eliminating two couplers and three phase shifters compared to the traditional 3×3 NM. To accommodate the hexagonal structure of the six-port coupler, the input ports (Ports 1–3) and output ports (Ports 4–6) are no longer symmetrically distributed on the left and right sides. Compared to the conventional NM, the components are reduced from six to one.

The following phase distribution is exhibited by a six-port coupler with a centrally symmetric regular hexagonal structure: $\angle S_{43} = \angle S_{51} = \angle S_{62} = \theta_1, \angle S_{41} = \angle S_{51} = \angle S_{42} = \angle S_{52} = \angle S_{53} = \angle S_{63} = \varphi_1$ and equal amplitude

$|S_{j1}| = |S_{j2}| = |S_{j3}|$ ($j = 4, 5, \text{ or } 6$). The scattering matrix of the proposed 3×3 BFN with input Ports 1–3 and output Ports 4–6 can be expressed as

$$S = \begin{bmatrix} O & A \\ A^T & O \end{bmatrix} \quad (2)$$

where O is the 3×3 zero matrix, and

$$A = \begin{bmatrix} e^{j\varphi_1} & e^{j\theta_1} & e^{j\varphi_1} \\ e^{j\varphi_1} & e^{j\varphi_1} & e^{j\theta_1} \\ e^{j\theta_1} & e^{j\varphi_1} & e^{j\varphi_1} \end{bmatrix}. \quad (3)$$

The lossless condition $U = S \cdot S^+$ can be used to derive the following equation [24], where S^+ denotes the Hermitian transpose of S :

$$U_{12} = \frac{1}{3} (1 + e^{j(\theta_1 - \varphi_1)} + e^{j(\varphi_1 - \theta_1)}) = 0. \quad (4)$$

While the condition $\varphi_1 - \theta_1 = \pm 2\pi/3$ is fulfilled, (4) is valid. However, this result does not meet the phase distribution of (1). For a satisfied output phase, change $\angle S_{62} = \theta_1 + \varphi_a$ to fulfill the following conditions:

$$\begin{cases} \angle S_{41} - \angle S_{51} = \angle S_{51} - \angle S_{61} = \pm \frac{2\pi}{3} \\ \angle S_{42} - \angle S_{52} = \angle S_{52} - \angle S_{62} = 0 \\ \angle S_{43} - \angle S_{53} = \angle S_{53} - \angle S_{63} = \mp \frac{2\pi}{3} \end{cases} \quad (5)$$

gives

$$\begin{cases} \varphi_a = \varphi_1 - \theta_1 \\ \varphi_1 - \theta_1 = -\frac{2\pi}{3} \end{cases} \quad (6)$$

Bring (6)–(3), there is

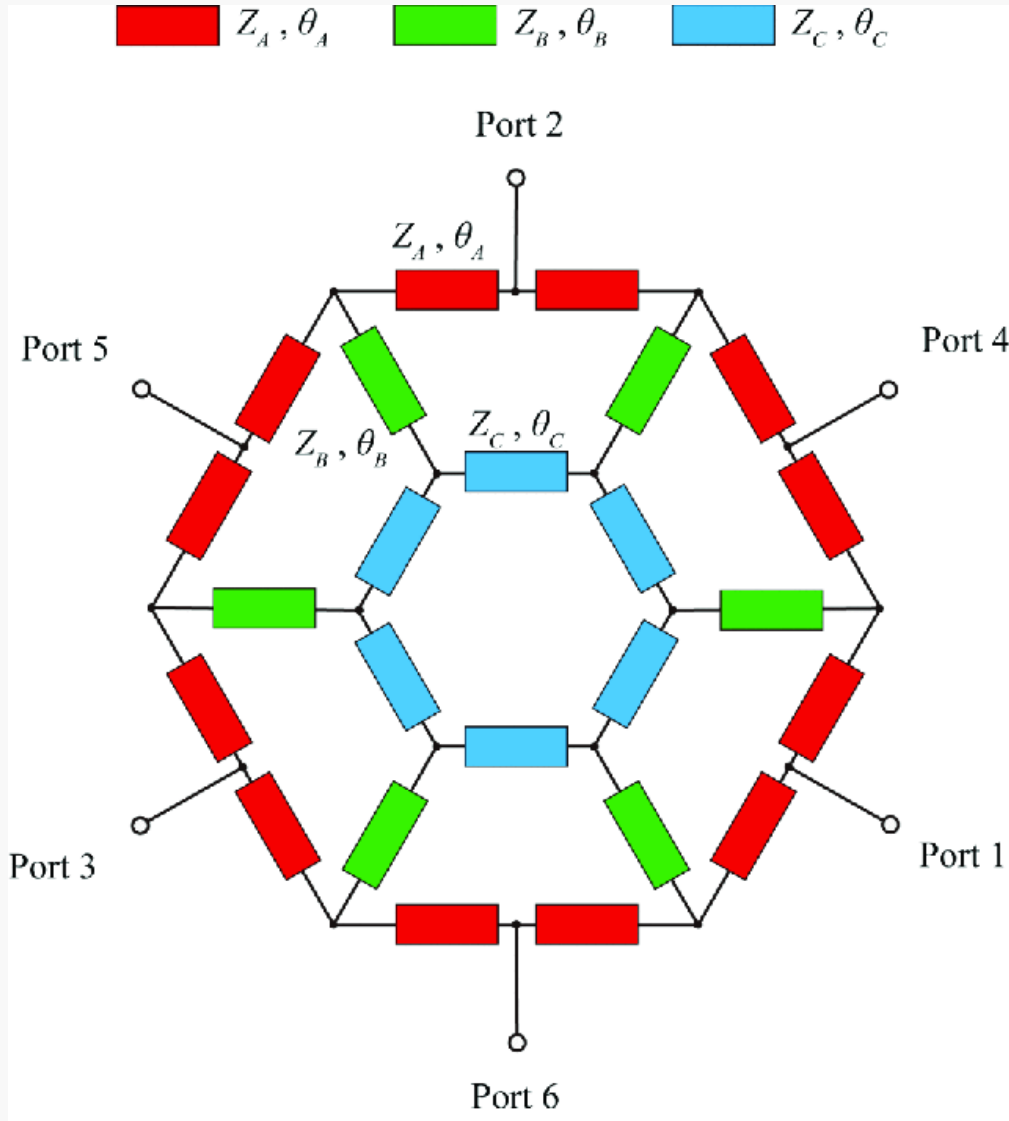
$$A_a = \begin{bmatrix} 1 & e^{j\frac{2\pi}{3}} & e^{-j\frac{2\pi}{3}} \\ 1 & 1 & 1 \\ 1 & e^{-j\frac{2\pi}{3}} & e^{j\frac{2\pi}{3}} \end{bmatrix}. \quad (7)$$

Similar to (1), the phase difference between each element in a row and its adjacent subsequent element is -120° , 0° , and 120° , respectively. By introducing the extra phase φ_a at Port 6, the proposed six-port hybrid coupler realizes the function of a 3×3 NM for multibeam scanning. As a result, the number of components can be reduced from six to one, significantly simplifying the complexity of the uniplanar six-port hybrid coupler.

III. Design of Six-Port Hexagonal Couplers

Based on the above analysis, this section will introduce two designs of six-port couplers with equal and unequal power division. The proposed six-port coupler consists of two regular hexagons with overlapping centers and connecting branches between them, as shown in Fig. 2. The power at each output port can be controlled by the impedance of the transmission lines so that unequal power division among output ports can be realized. This section will present explicit equations utilizing the even- and odd-mode analysis to determine the relevant parameters according to a given power division ratio. The uniplanar six-port hexagonal couplers are designed at the center frequency of 2.45 GHz, using RO4350B substrate with a dielectric constant of 3.48 and a loss tangent of 0.0037 at 10 GHz. The conductor layer is made of copper with a thickness of 0.018 mm and a gold-immersed surface.

Fig. 2. Schematic of the proposed six-port hexagonal coupler (for simplicity in analysis, the extra phase φ_a at Port 6 has been omitted).



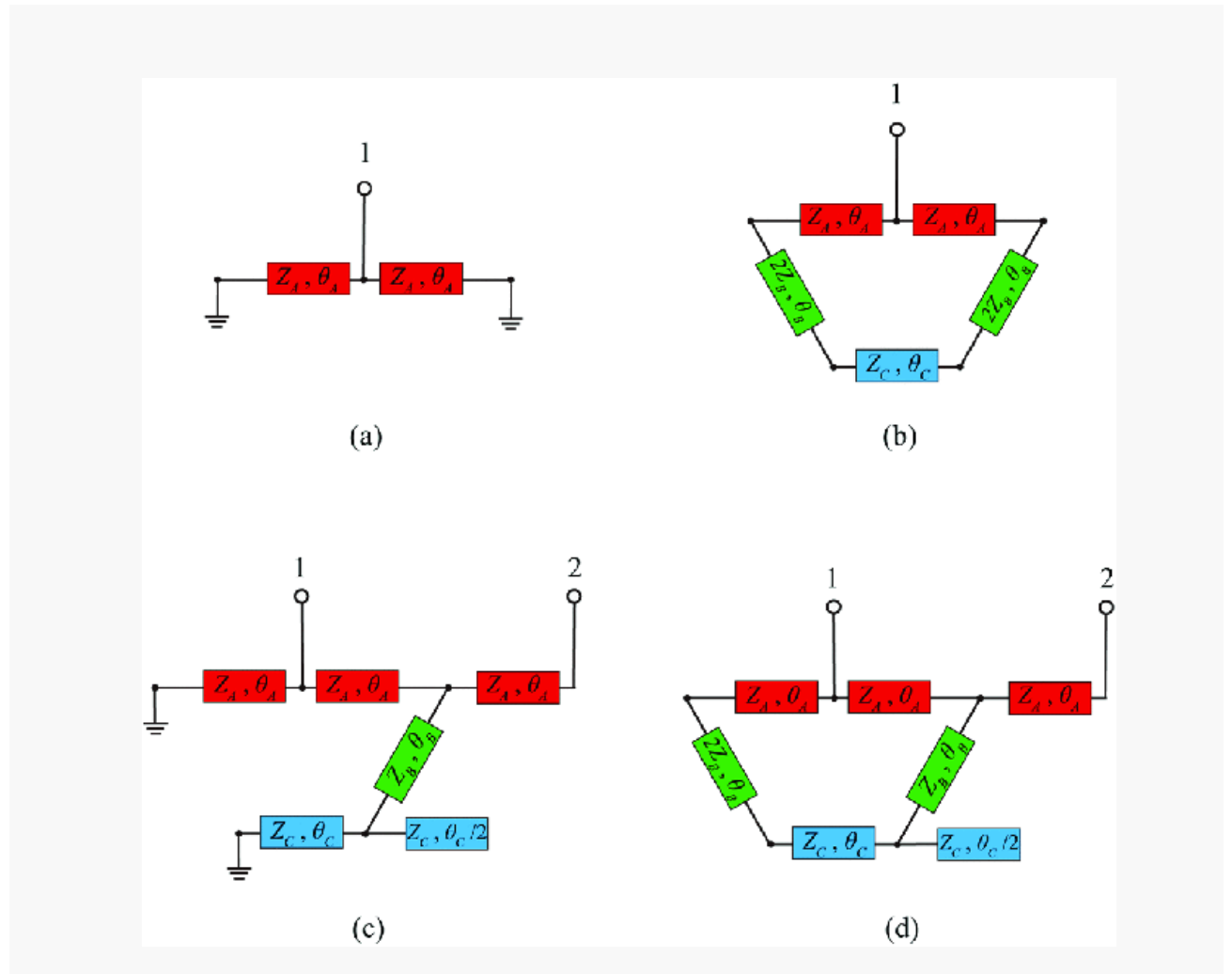
A. Theoretical Equation

As seen from Fig. 2, z_A and θ_A refer to the unilateral resistances and electrical lengths of the outermost ring hexagon, respectively. z_B and θ_B are the unilateral resistances and electrical lengths of the inner regular hexagon ring, respectively. The impedance and electrical length of the intermediate connecting branches are divided by z_C and θ_C . Considering the network's symmetry and combinatorial excitation characteristics, electric and magnetic walls are added to the network. As shown in Fig. 3,

depicting branch equivalent circuits, the six-port network is converted into several single-port or dual-port subnetworks. According to [30], for the input reflection coefficient Γ_i (including Γ_{odd} , Γ_{even} , Γ_{oe} , and Γ_{ee}) can be expressed as

$$\Gamma_i = \frac{1 - Y_i Z_0}{1 + Y_i Z_0}. \quad (8)$$

Fig. 3. Partial equivalent circuits of the six-port hexagonal coupler with different excitation: (a) Odd–odd, (b) even–even–even, (c) odd–even, and (d) even–even.



Here, Y_i , including Y_{ooo} , Y_{ooo} , Y_{oe} , and Y_{ee} , represents the input port admittances of the equivalent circuit, and Z_0 is the impedance of the six ports. According to Fig. 3(a), the input admittance Y_{ooo} is obtained as

$$Y_{ooo} = -j \frac{2}{Z_A} \cot \theta_A. \quad (9)$$

In Fig. 3(b), it is considered as two secondary open circuits separated by a magnetic wall because it features a symmetric single-port network. Then, the input admittance Y_{ees} is expressed as

$$Y_{ees} = \frac{2(Z_A Y_{m1} + j \tan \theta_A)}{Z_A (1 + Z_A j Y_{m1} \tan \theta_A)} \quad (10)$$

$$Y_{m1} = j \frac{2Z_B + Z_C \tan \theta_B \cot \frac{\theta_C}{2}}{2Z_B (Z_C \cot \frac{\theta_C}{2} - 2Z_B \tan \theta_B)}. \quad (11)$$

The input admittance Y_{oe} in Fig. 3(c), representing a two-port π -type network, can be determined by

$$Y_{oe} = j \frac{4 \cos^2 \theta_A - Z_A Y_{m2} \sin 2\theta_A - 3}{Z_A \sin \theta_A (Z_A Y_{m2} \sin \theta_A - 2 \cos \theta_A)} \quad (12)$$

$$Y_{m2} = \frac{1}{Z_B} \frac{Z_B (1 - 2 \cos \theta_C) \cos \theta_B + Z_C \sin \theta_B \sin \theta_C}{Z_C \sin \theta_C \cos \theta_B - Z_B (1 - 2 \cos \theta_C) \sin \theta_B}. \quad (13)$$

The asymmetric two-port network, shown in Fig. 3(d), is a key component of the overall structure. Following the node-analysis method outlined in [31], the even-even mode characteristic admittance Y_{ee} is derived as (14)–(18) shown at the bottom of this page.

$$Y_{ee} = \frac{Y_{m6} (1 + 2 \cos 2\theta_A) + Z_A j \sin \theta_A [Y_{m3} Y_{m4} + 2 \cos \theta_A (Y_{m5} Y_{m6} - Y_{m3}^2)]}{Z_A \sin \theta_A^2 [Z_A (Y_{m3}^2 - Y_{m5} Y_{m6}) + 2j Y_{m6} \cot \theta_A]} \quad (14)$$

$$Y_{m3} = j \frac{1}{Z_B \sin \theta_B \cos \theta_C + Z_C \cos \theta_B \sin \theta_C} \quad (15)$$

$$Y_{m4} = j \frac{1}{Z_A \sin \theta_A \cos \theta_B + 2Z_B \cos \theta_A \sin \theta_B} \quad (16)$$

$$Y_{m5} = -j \frac{Z_B \cos \theta_B \cos \theta_C - Z_C \sin \theta_B \sin \theta_C}{Z_B (Z_B \sin \theta_B \cos \theta_C + Z_C \cos \theta_B \sin \theta_C)} \quad (17)$$

$$Y_{m6} = -j \frac{2Z_B \cos \theta_A \cos \theta_B - Z_A \sin \theta_A \sin \theta_B}{2Z_B (Z_A \sin \theta_A \cos \theta_B + 2Z_B \cos \theta_A \sin \theta_B)} - j \frac{Z_C \cos \theta_B (\cos \theta_C - \tan \frac{\theta_C}{2} \sin \theta_C) - Z_B \sin \theta_B (\sin \theta_C + \tan \frac{\theta_C}{2} \cos \theta_C)}{Z_C (Z_B \sin \theta_B \cos \theta_C + Z_C \cos \theta_B \sin \theta_C)} \quad (18)$$

In addition, the six-port hexagonal coupler under consideration comprises two regular hexagonal rings sharing a common center point. Branch lines connect the outer vertices of the inner hexagonal ring to the inner vertices of the outer hexagonal ring. Therefore, the following relationship can be obtained:

$$\begin{cases} \theta_A = N\theta_C \\ \theta_B = (2N - 1)\theta_C \end{cases} \quad (19)$$

where the N is a rational number close to 1.

Then, the s -parameters of the six-port coupler can be expressed as

$$S_{11} = \frac{1}{6}(\Gamma_{ooo} + 2\Gamma_{oe} + 2\Gamma_{ee} + \Gamma_{eee}) \quad (20)$$

$$S_{21} = S_{31} = \frac{1}{6}(\Gamma_{ooo} - \Gamma_{oe} - \Gamma_{ee} + \Gamma_{eee}) \quad (21)$$

$$S_{41} = S_{51} = \frac{1}{6}(\Gamma_{ooo} - \Gamma_{oe} + \Gamma_{ee} - \Gamma_{eee}) \quad (22)$$

$$S_{61} = \frac{1}{6}(\Gamma_{ooo} - 2\Gamma_{oe} + 2\Gamma_{ee} - \Gamma_{eee}). \quad (23)$$

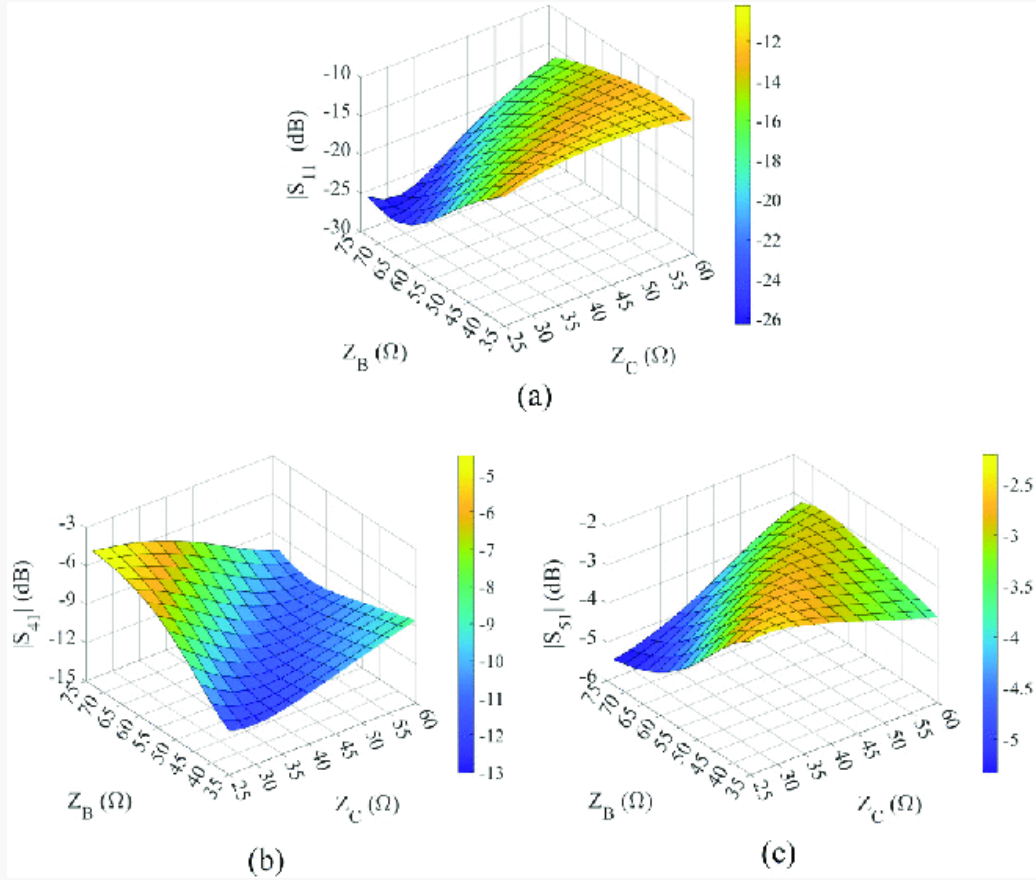
Substituting (8)–(18) to (20)–(23), relevant parameters can be found to meet the expected performance metrics of the six-port regular hexagonal coupler. These metrics include ideal input return loss and port-to-port isolation, controllable output power-division ratio, and the predetermined phase difference between three output ports. In addition, the performance characteristics of the other ports are similar to those of Port 1 due to the reciprocity of the proposed six-port circuit.

B. Design of Equal Six-Port Regular Hexagonal Coupler

This section aims to design a six-port regular hexagonal coupler with equal power division at output ports (1:1:1) and phase difference of -120° , 0° , and 120° when three inputs are excited, which is the same characteristics as the normal NM. Based on the theoretical analysis and the symmetrical characteristics outlined above, the parameters in the six-port coupler depicted in Fig. 2, namely, Z_A, θ_A, Z_B, Z_C , and N , can be obtained. In order to simplify the design process and constrain the physical dimensions, the values of Z_A and θ_A ($60\ \Omega$ and 55° are typically employed in a conventional ring coupler) are fixed in advance in the proposed designs. This makes it possible to derive the remaining unknown parameters.

Fig. 4 illustrates the design diagrams for Z_B and Z_C at the center frequency with $N = 1$. To achieve the target power division, where $|S_{41}|, |S_{51}|$, and $|S_{61}|$ approximate $-4.77\ \text{dB}$, the required impedances of Z_B and Z_C fall within the ranges of $68\text{--}72\ \Omega$ and $26\text{--}32\ \Omega$, respectively. By referencing the return loss curve, the value of Z_B and Z_C for the six-port coupler with NM matrix functionality are identified as $70\ \Omega$ and $30\ \Omega$, respectively.

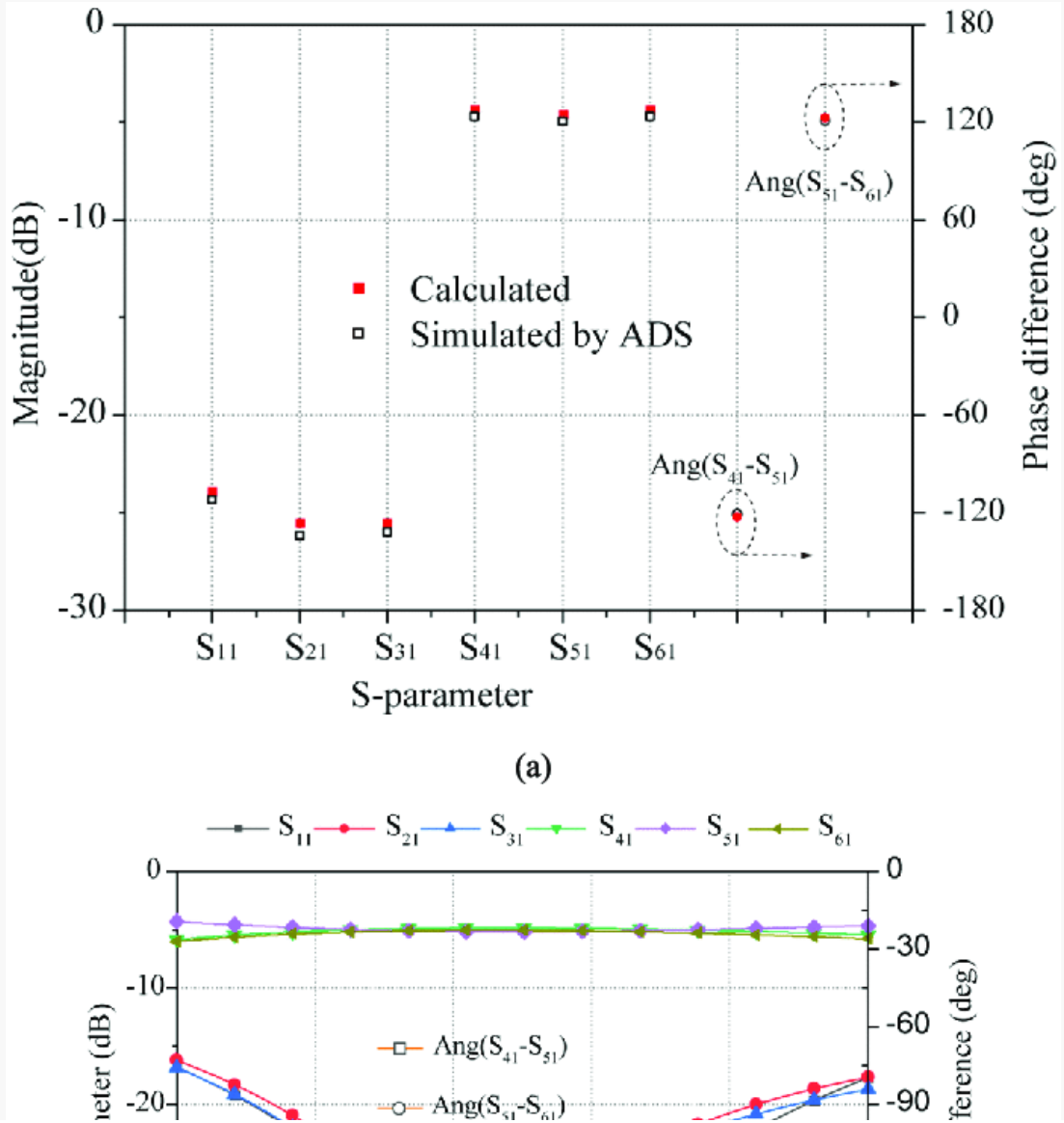
Fig. 4. Design diagrams [AQ3](#) of the proposed coupler with different z_B and z_C .

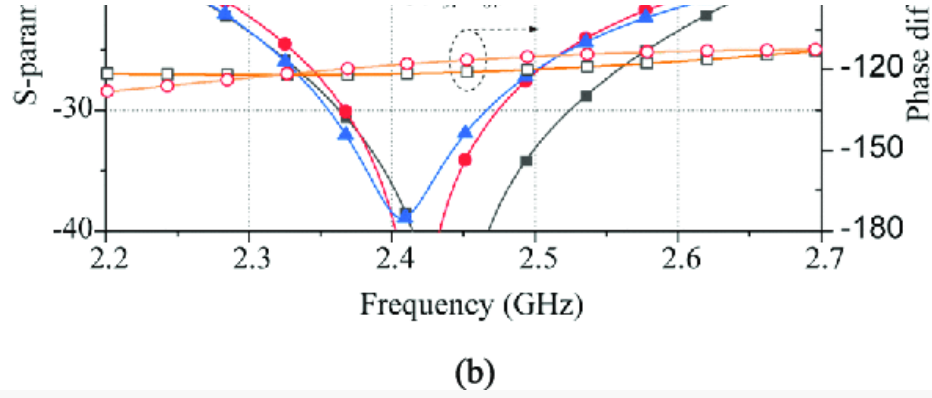


To quickly verify the calculated results, the derived parameters were implemented in ADS for simulation. The comparison result between calculated and simulated s -parameters at 2.45 GHz is provided in [Fig. 5\(a\)](#). Based on the calculated electrical parameters and the RO4350B substrate properties, the corresponding physical dimensions were derived to form the initial coupler layout. To account for practical structural effects, including discontinuities at π -junctions and parasitic coupling between transmission lines, the layout was further optimized through rigorous full-wave electromagnetic simulations using CST. The final simulated performance is presented in [Fig. 5\(b\)](#).

The return loss and isolation exceed 21 and 20.7 dB, respectively, across the 2.28–2.61-GHz band. In addition, the transmission coefficient remains within 5 ± 0.38 dB, while the phase differences at Port 1 are maintained at $-120^\circ \pm 9^\circ$.

Fig. 5. Performance of the proposed coupler with equal power division. (a) Comparison results between the calculated and ADS. (b) Simulated results in CST with extra phase φ_0 at Port 6.





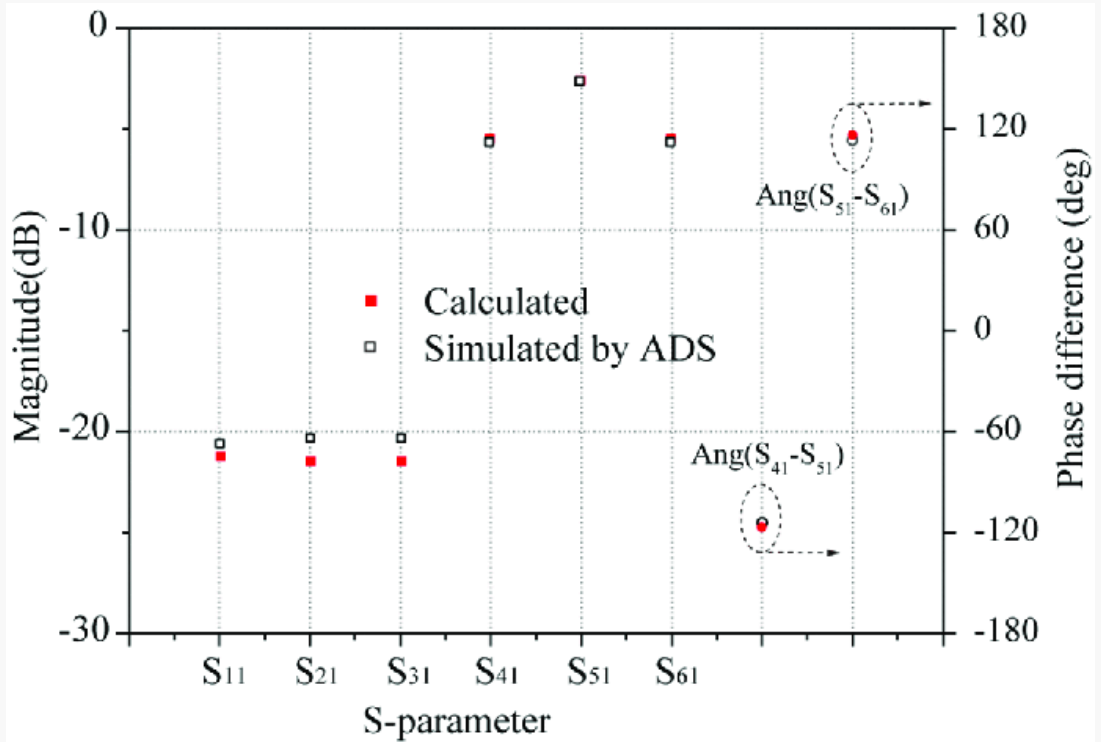
C. Design of Unequal Six-Port Regular Hexagonal Coupler

While the aforementioned equal-power-division six-port coupler demonstrates ideal performance in theoretical analysis and for symmetric applications, an unequal power division is often advantageous in practical scenarios. To broaden the coupler's applicability and improve its measurement accuracy under such asymmetric conditions, the design methodology is extended from the equal power-division case to the unequal one. The following [AQ4](#) section details the systematic design procedure for achieving an arbitrary power division ratio.

The arbitrary power division of the six-port hexagonal coupler will be obtained by (20)–(23). And the related output phase difference is calculated by (3)–(6). In this section, another six-port hexagonal coupler is realized based on a similar structure and the aforementioned method. According to the same initial conditions, $z_A = 60 \Omega$ and $\theta_A = 55^\circ$, a six-port hexagonal coupler with the power division of 1:2:1 is targeted. The analysis of the equal-power-division case, as illustrated in Fig. 4, reveals the relationship between the impedances z_B and z_C , and performance metrics. Specifically, the output power at Port 5 decreases as z_C increases and increases as z_B decreases, respectively. Similarly, the output power at Port 4 increases as z_C increases and decreases as z_B decreases, respectively. Leveraging this insight to simplify the design process, the value of z_C is fixed at 30Ω . Subsequently, the remaining unknown parameters, z_B and N , are calculated to satisfy the desired power division. When the value of z_A, θ_A , and z_C is ensured, it is easy to obtain the design diagrams for the unequal-power-division coupler with the variable z_B and N . The following steps for calculating specific values are similar to those outlined in the aforementioned section and will not be repeated here. Finally, the

value of z_B and N for the six-port coupler with a 1:2:1 power division are identified as $50\ \Omega$ and 1.22, respectively. And the comparison result between calculated and simulated s -parameters at 2.45 GHz is provided in Fig. 6 to validate the design process.

Fig. 6. Comparison between calculated and simulated performance of the proposed coupler with unequal power division.



The design of both equal and unequal-power regular hexagonal six-port couplers can be obtained through the following steps.

1. Set an arbitrary power division and output phase division as the specific design goal. Based on these phase requirements, the electrical lengths of the special transmission lines are calculated using the design equations in (3)–(6).

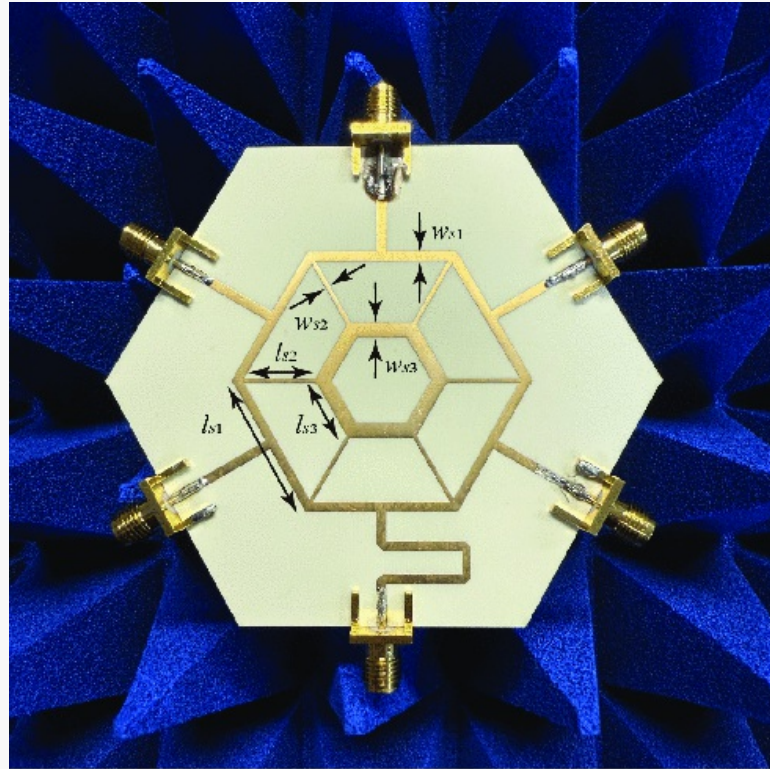
2. Predetermine key initial parameters based on conventional values or previous analysis to constrain the design space and simplify the problem. For instance, z_A and θ_A are set as initial values. N may be initialized to 1.
3. Plot the design diagram of the variable z_B and z_C according to (8)–(23). Then, find the relationship between the variable and the performance metrics. Determine the value of the z_B and z_C with the aim of power division. Subsequently, the final dimensions may be adjusted by N .
4. Build the electromagnetic model and find its physical dimensions by the calculated electrical parameters based on the chosen substrate's properties. This forms the initial physical layout of the coupler.
5. Conduct a simulation of the EM model in a full-wave simulation software tool, such as CST. The structure is then rigorously optimized to account for practical structure effects, such as unavoidable discontinuities at T -junctions and parasitic coupling between transmission lines. This ensures the final design meets the required specifications with high accuracy.

IV. Experiment and Measurement Result

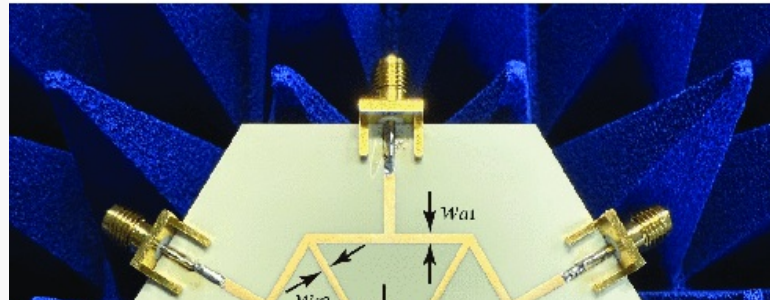
To validate the proposed design, two six-port regular hexagonal couplers operating at a center frequency of 2.45 GHz are implemented and tested: one with equal power division and the other with unequal power division. A Keysight vector network analyzer (N5225B) is employed to measure the S -parameters and output phase differences of the following prototypes. As illustrated in Fig. 7(a), the final dimensions of this six-port regular hexagonal coupler are given as follows: $l_{a1} = 24.26$ mm, $l_{a2} = 11.64$ mm, $l_{a3} = 10$ mm, $w_{a1} = 1.56$ mm, $w_{a2} = 0.7$ mm, and $w_{a3} = 2.38$ mm. The length of the phase delay line used to introduce a 120° phase difference is 23 mm. The comparison of simulated and measured results is presented in Fig. 8. According to Fig. 8(a) and (e), the simulated return loss and isolation are better than 21 and 20.7 dB from 2.28 to 2.61 GHz, respectively. The measured return loss and isolation are greater than 21.6 and 18.8 dB from 2.28 to 2.61 GHz, respectively. According to Fig. 8(b)–(d), the simulated transmission coefficient is -5 ± 0.38 dB within the operating band. And the measured transmission coefficient of Ports 1–3 is -5 ± 0.9 dB, -5 ± 0.76 dB, and -5 ± 0.6 dB within the operating band, respectively. According to Fig. 7(f)–(h), the simulated phase differences are $-120^\circ \pm 9^\circ$, $0^\circ \pm 11.7^\circ$, and $120^\circ \pm 9^\circ$. The measured phase differences are $-120^\circ \pm 10^\circ$, $0^\circ \pm 14^\circ$, and $120^\circ \pm 11^\circ$ from 2.28 to 2.61 GHz. The

measured results align closely with simulations, demonstrating the robustness of the symmetric design. The high phase error is primarily caused by the simple phase delay line. This error can be minimized by using a phase shifter with a precise phase difference.

Fig. 7. Prototype of the six-port regular hexagonal coupler. (a) With equal power division. (b) With unequal power division.



(a)



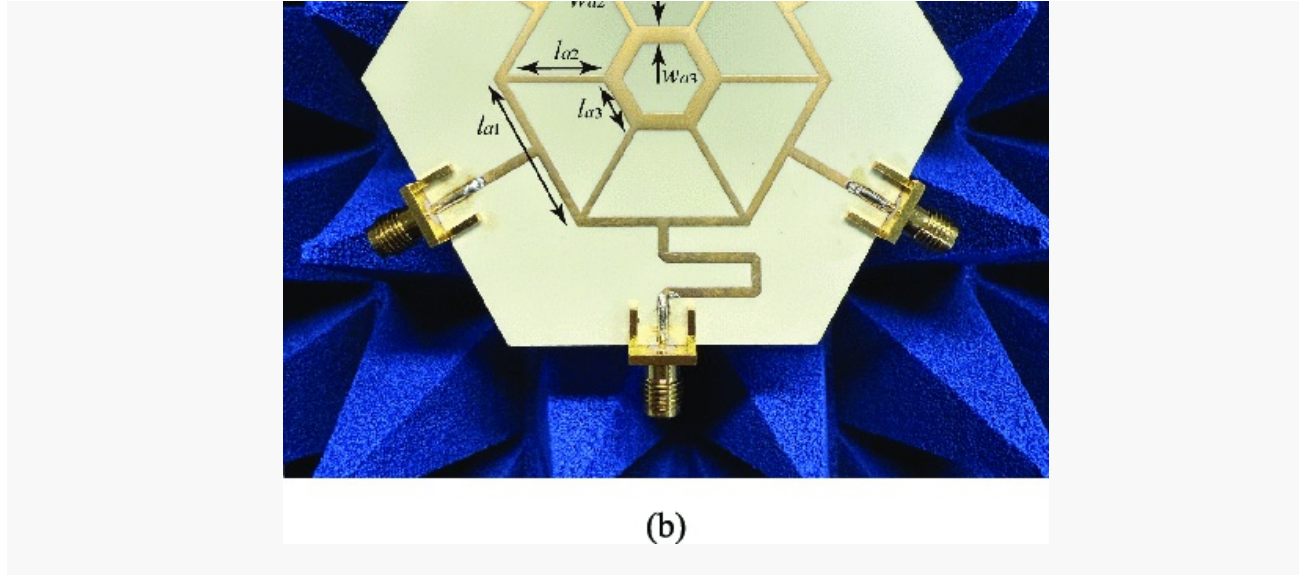
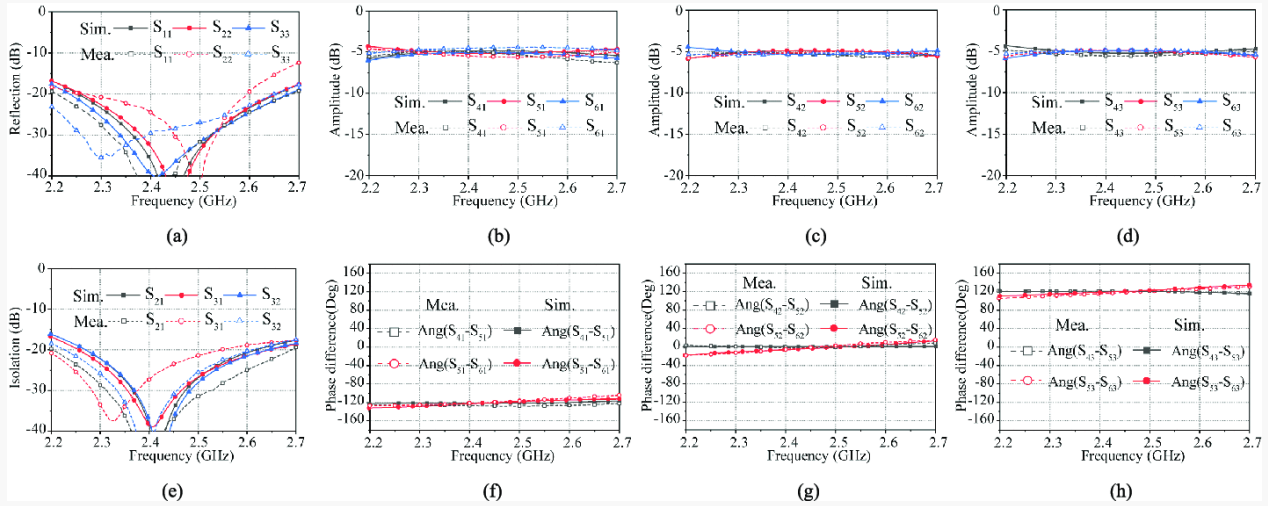


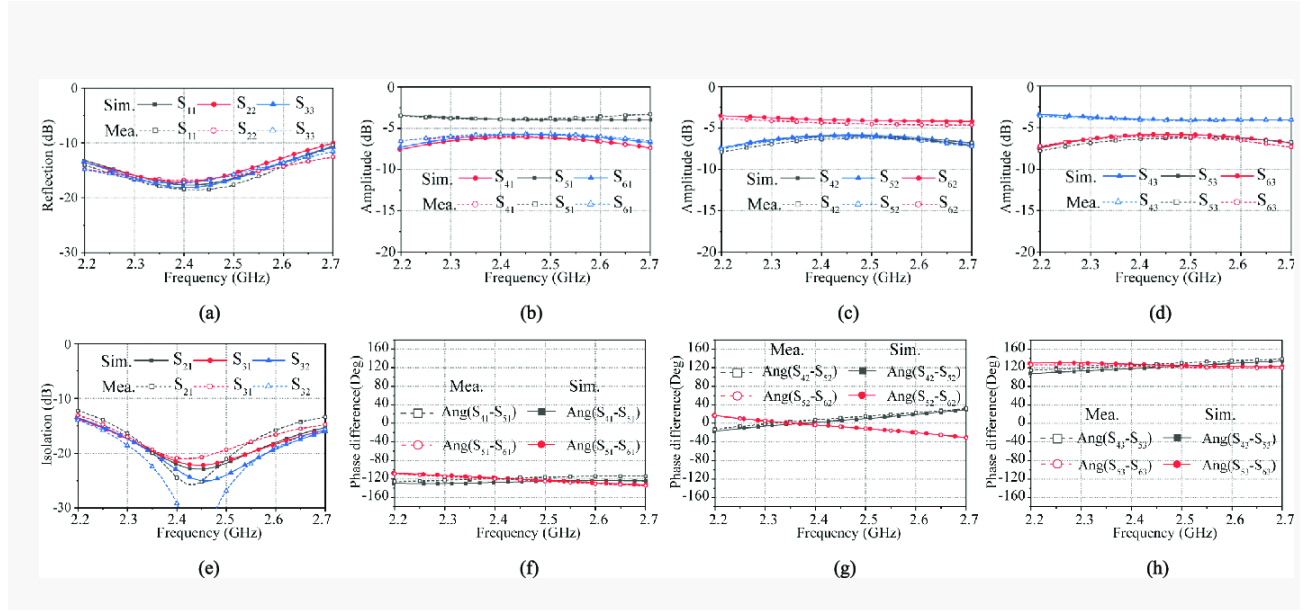
Fig. 8. Simulated and measured results of the proposed coupler with equal power division. (a) Reflection coefficient. (b)–(d) Transmission coefficient. (e) Isolation. (f)–(h) Output phase difference.



For the unequal power division case, another prototype of the six-port hexagonal coupler operating at a center frequency of 2.45 GHz with unequal power division is also implemented and measured.

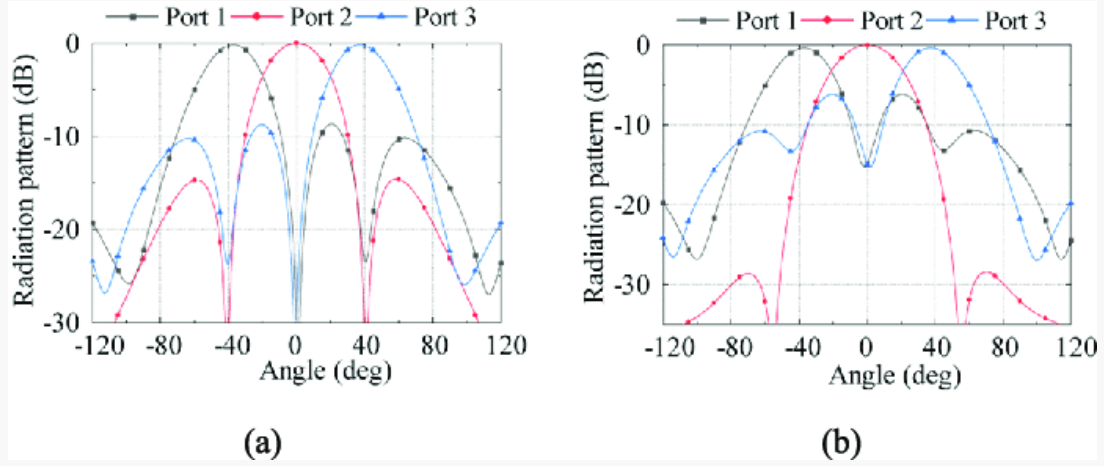
The final dimension of this BNF is shown in Fig. 7(b): $l_{a1} = 25.2$ mm, $l_{a2} = 14.55$ mm, $l_{a3} = 7.78$ mm, $w_{a1} = 1.39$ mm, $w_{a2} = 1.1$ mm, and $w_{a3} = 2.51$ mm. The length of the phase delay line used to add a 120° phase difference is also 23 mm. The comparison of simulated and measured results is shown in Fig. 9. According to Fig. 9(a) and (e), the simulated return loss and isolation are better than 12.7 and 16.95 dB from 2.3 to 2.6 GHz, respectively. The measured return loss and isolation are better than 13.6 and 15.8 dB from 2.3 to 2.6 GHz, respectively. According to Fig. 9(b)–(d), the simulated transmission coefficient is 3.7 ± 0.3 dB and 6.1 ± 0.37 dB within the operating band. The measured transmission coefficient is 3.7 ± 1 dB and 6.1 ± 0.9 dB within the operating band, respectively. According to Fig. 9(f)–(h), the simulated phase differences are $-120^\circ \pm 10^\circ$, $0^\circ \pm 20^\circ$, and $120^\circ \pm 10^\circ$. The measured phase differences are $-120^\circ \pm 10^\circ$, $0^\circ \pm 23^\circ$, and $120^\circ \pm 14^\circ$ from 2.3 to 2.6 GHz. The significant error is mainly attributed to the basic phase delay line, which can be minimized by employing a phase shifter with a precise phase difference. The unequal power ratio design exhibits slightly degraded performance compared to the symmetric case, particularly in phase consistency, due to the inherent complexity of nonuniform power distribution. Furthermore, the restrictions on bandwidth, isolation, and insertion loss will increase as the power allocation ratio becomes more extreme.

Fig. 9. Simulated and measured results of the proposed coupler with unequal power division. (a) Reflection coefficient. (b)–(d) Transmission coefficient. (e) Isolation. (f)–(h) Output phase difference.



The simulated normalized radiation patterns of a 1×3 array at 2.45 GHz with element spacing of half wavelength fed by different six-port couplers are shown in Fig. 10. As shown in Fig. 10(a), the beam scan angles are -37° , 0° , and 37° for Ports 1–3, respectively. Similarly, the beam scan angles are 36.8° , 0° , and 37° for Ports 1–3 in Fig. 10(b), respectively.

Fig. 10. Simulated normalized radiation patterns of a 1×3 array at 2.45 GHz with element spacing of half wavelength fed by different six-port couplers. (a) Coupler with equal power division. (b) Coupler with unequal power division.



The detailed comparison between these two six-port hexagonal couplers and other works on 3×3 BFN or three-way couplers is presented in Table I. Most reports, which typically exhibit equal power division ratios, involve nonplanar structures consisting of coupling lines, striplines, and SIW structures. [16], [18], [20] describe cascaded structures comprising either equal or unequal power division couplers and phase shifters with precise phase differences. These configurations offer the advantages of wideband and outstanding phase fluctuation but are constrained by their large size and complex design requirements. Compared to previous works, the primary innovation of our design is the implementation of each 3×3 BFN using only a single compact hexagonal coupler. Furthermore, in contrast to similar three-way directional couplers in [24] and [28], the proposed designs feature a fully uniplanar structure. The size of these two six-port regular hexagonal couplers is both $2.59 \times 0.37\lambda_0^2$, where $0.37\lambda_0$ represents the side length of this hexagonal shape, respectively. The insertion loss is lower due to the compact size; however, the unequal power distribution introduces extra loss in design II. Overall, the results demonstrate that the proposed six-port hexagonal couplers achieve a balance between compactness, planar integration, and performance, making them suitable for large-scale BFN topologies and compact, scalable beamforming systems.

Note: The table layout displayed in 'Edit' view is not how it will appear in the printed/pdf version. This html display is to enable content corrections to the table. To preview the printed/pdf presentation of the table, please view the 'PDF' tab.

TABLE I Comparison With Other Similar Works With a 3×3 BFN Function

Ref	FR (GHz)	Structure	PDR	Planarity	CNB	IL (dB)	AF (dB)	PF (deg)	BW (%)	Size (λ_0^3)
[16] (Sim.)	2.2	Stripline	Equal	Not planar	6	0.33	0.7	10	45	NA
[18] (Mea.)	1.75	Microstrip	Equal	Not planar	7	2.2	10	5	46	$0.35 \times 0.45 \times 0.03$ (4.73×10^{-3})
[20] (Mea.)	3.5	Microstrip	Equal	Uniplanar	5	0.2	0.5	5	34.3	$4.92 \times 6.6 \times 0.05$ (1.62)
[22] (Mea.)	4.05	Microstrip	Equal	Not planar	5	2	9	5	30	$0.75 \times 1.5 \times 0.01$ (0.01)
[23] (Mea.)	28	SIW	Equal and Unequal*	Not planar	3	0.86	2.5	12	4.1	$5.65 \times 5.65 \times 23.02$ (734.9)
[24] (Mea.)	5.8	Microstrip	Equal	Not planar	1	0.8	1.3	14	7	$0.97 \times 0.87 \times 0.0003$ (2.53×10^{-4})
[28] (Sim.)	28	SIW	Equal	Not planar	1	0.3	0.7	NA	7.1	$1 \times 1.5 \times 0.14$ (0.21)
Design 1 (Mea.)	2.45	Microstrip	Equal	Uniplanar	1	0.23	0.9	14	13	$1.46 \times 1.46 \times 0.0006$ (2.13×10^{-4})
Design 2 (Mea.)	2.45	Microstrip	Unequal [#]	Uniplanar	1	0.7/0.1	1/0.9	20	10	$1.46 \times 1.46 \times 0.0006$ (2.13×10^{-4})

PDR: Power division ratio, CNB: Components number of BFN, IL: Insertion loss, AF: Amplitude fluctuations, PF: Phase fluctuations, BW: bandwidth


V. Conclusion


In this article, a novel six-port hexagonal coupler is presented for multibeam applications. The design integrates multiple couplers and phase shifters into a single planar structure, greatly simplifying the conventional NM. Two prototypes with equal and unequal power division were designed, fabricated, and measured. Both demonstrate excellent performance in terms of transmission, return loss, isolation, and phase stability. The equal-division coupler provides three output signals with identical magnitudes, while the unequal-division version enables flexible power distribution for advanced beamforming. The dimensions of these two six-port regular hexagonal couplers are both $2.59 \times 0.37 \lambda_0^2$, respectively. Owing to its compact size and planar configuration, the proposed coupler is highly suitable for modern wireless systems such as MIMO and multibeam antenna arrays. Future research may explore its integration into larger array architectures and further miniaturization to enhance applicability in next-generation communication networks.


Note: this Edit/html view does not display references as per your journal style. There is no need to correct this. The content is correct and it will be converted to your journal style in the published version.


References


- [1] A. N. Atanasov, M. S. O. Alink, and F. E. van Vliet, "A figure of merit for simultaneous-multi-beam transmit antenna arrays," *IEEE Trans. Radar Syst.*, vol. 1, pp. 60–68, 2023. 
- [2] C. Geng, J.-W. Lian, Y. J. Guo, and D. Ding, "Millimeter-wave three-layer substrate-integrated 9×9 Butler matrix and its application to wide-angle endfire multibeam metasurface antenna," *IEEE Trans. Microw. Theory Techn.*, vol. 72, no. 4, pp. 2253–2266, Apr. 2024. [AQ5](#) 
- [3] J. Hirokawa and N. J. G. Fonseca, "Generalized one-dimensional parallel switching matrices with an arbitrary number of beams," *IEEE J. Microw.*, vol. 1, no. 4, pp. 975–988, Oct. 2021. 
- [4] T. Djerafi, N. J. G. Fonseca, and K. Wu, "Planar Ku-band 4×4 nolen matrix in SIW technology," *IEEE Trans. Microw. Theory Techn.*, vol. 58, no. 2, pp. 259–266, Feb. 2010. 
- [5] H. Liu, X. Gu, and H. Tian, "Design of extended nolen matrix with enhanced beam controllability and widened spatial coverage," *IEEE Trans. Circuits Syst. II, Exp. Briefs*, vol. 71, no. 7, pp. 3273–3277, Jul. 2024. 
- [6] M. O. Shady and A. A. Kishk, "Compact 4×4 multilayer Butler matrix with four-slot array," *IEEE Trans. Microw. Theory Techn.*, vol. 72, no. 6, pp. 3522–3529, Jun. 2024. 
- [7] H. Zhu, P.-Y. Qin, and Y. J. Guo, "Single-ended-to-balanced power divider with extended common-mode suppression and its application to differential 2×4 Butler matrices," *IEEE Trans. Microw. Theory Techn.*, vol. 68, no. 4, pp. 1510–1519, Apr. 2020. 
- [8] W. Sun, X. Rao, G. Su, L. Sun, C. Shu, and X. Chen, "A miniaturized wideband 4×8 Butler


matrix for beamforming in millimeter-wave applications,” *IEEE Trans. Microw. Theory Techn.*, vol. 71, no. 10, pp. 4588–4599, Oct. 2023. 


[9] C. Geng, J.-W. Lian, and D. Ding, “Millimeter-wave highly efficient E-plane ridge gap waveguide Butler matrix for wide-angle endfire multibeam antenna applications,” *IEEE Trans. Microw. Theory Techn.*, vol. 73, no. 8, pp. 5096–5107, Aug. 2025. 


[10] H. Ding, F. Lin, Z. Yin, Y. Yang, and H. Sun, “Additively manufactured broadband miniaturized quadrature coupler and its application to 2-D scanning broadband Butler matrix,” *IEEE Trans. Microw. Theory Techn.*, vol. 73, no. 9, pp. 5803–5812, Sep. 2025. 


[11] Z. Yin, Y. Yang, and H. Zhu, “Multi-material additively manufactured wideband millimeter-wave Butler matrix,” in *IEEE MTT-S Int. Microw. Symp. Dig.*, Wuxi, China, Jul. 2025, pp. 1–3. 

[12] Z. Yin, H. Zhu, X. Lv, J. Lai, and Y. Yang, “3-D-printed ultracompact Butler matrix for wideband millimeter-wave beamforming,” *IEEE Trans. Microw. Theory Techn.*, vol. 73, no. 9, pp. 5953–5965, Sep. 2025. 

[13] C. A. Guo, Y. J. Guo, H. Zhu, W. Ni, and J. Yuan, “Optimization of multibeam antennas employing generalized joined coupler matrix,” *IEEE Trans. Antennas Propag.*, vol. 71, no. 1, pp. 215–224, Jan. 2023. 


[14] C. Tsokos *et al.*, “Analysis of a multibeam optical beamforming network based on Blass matrix architecture,” *J. Lightw. Technol.*, vol. 36, no. 16, pp. 3354–3372, Aug. 15, 2018. 


[15] C. A. Guo and Y. J. Guo, “A general approach for synthesizing multibeam antenna arrays employing generalized joined coupler matrix,” *IEEE Trans. Antennas Propag.*, vol. 70, no. 9, pp. 7556–7564, Sep. 2022. 


[16] H. Zhu, H. Sun, B. Jones, C. Ding, and Y. J. Guo, “Wideband dual-polarized multiple beam-forming antenna arrays,” *IEEE Trans. Antennas Propag.*, vol. 67, no. 3, pp. 1590–1604, Mar. 2019. 


[17] Y. J. Guo, M. Ansari, and N. J. G. Fonseca, “Circuit type multiple beamforming networks for


antenna arrays in 5G and 6G terrestrial and non-terrestrial networks,” *IEEE J. Microw.*, vol. 1, no. 3, pp. 704–722, Jul. 2021. 


[18] Y. Yang, Y. F. Pan, W. S. Chan, and S. Y. Zheng, “Dimension expansion method and implementation of broadband planar 2-D 3×3 nolen matrix,” *IEEE Trans. Antennas Propag.*, vol. 71, no. 9, pp. 7395–7408, Sep. 2023. 


[19] Y. Yang, Y. F. Pan, S. Y. Zheng, W. Hong, and W. S. Chan, “Analytical design method and implementation of broadband 4×4 nolen matrix,” *IEEE Trans. Microw. Theory Techn.*, vol. 70, no. 1, pp. 343–355, Jan. 2022. 

[20] Y. Xu, H. Zhu, and Y. J. Guo, “Compact wideband 3×3 nolen matrix with couplers integrated with phase shifters,” *IEEE Microw. Wireless Technol. Lett.*, vol. 34, no. 2, pp. 159–162, Feb. 2024. 

[21] H. Zhu, M. Ansari, and Y. J. Guo, “Wideband beam-forming networks utilizing planar hybrid couplers and phase shifters,” *IEEE Trans. Antennas Propag.*, vol. 70, no. 9, pp. 7592–7602, Sep. 2022. 


[22] H. Zhu, T. Zhang, and Y. J. Guo, “Wideband hybrid couplers with unequal power division/arbitrary output phases and applications to miniaturized nolen matrices,” *IEEE Trans. Microw. Theory Techn.*, vol. 70, no. 6, pp. 3040–3053, Jun. 2022. 

[23] Q. Li, J. Hirokawa, T. Tomura, and N. J. G. Fonseca, “Two-dimensional one-body 3×3-way hollow-waveguide nolen matrix using a two-plane unequal division coupler,” *IEEE Trans. Microw. Theory Techn.*, vol. 72, no. 1, pp. 376–390, Jan. 2024. 


[24] K. Ding, X. Fang, Y. Wang, and A. Chen, “Printed dual-layer three-way directional coupler utilized as 3×3 beamforming network for orthogonal three-beam antenna array,” *IEEE Antennas Wireless Propag. Lett.*, vol. 13, pp. 911–914, 2014. 


[25] K. Han, G. Wei, S. Lei, M. Wang, and T. Qiu, “Design of broadband 9×9 Butler matrix and its extension for multibeam application,” *IEEE Trans. Circuits Syst. II, Exp. Briefs*, vol. 70, no. 8, pp.


2874–2878, Aug. 2023. 


[26] Y. Yang, Y.-L. Ban, Q. Yang, J.-W. Lian, Q. Sun, and G. Wu, “Millimeter wave wide-angle scanning circularly polarized antenna array with a novel polarizer,” *IEEE Trans. Antennas Propag.*, vol. 70, no. 2, pp. 1077–1086, Feb. 2022. 

[27] K. Han, G. Wei, M. Wang, and T. Qiu, “Design and extension of modified Butler matrix based on three-way directional coupler and its multibeam application,” *IEEE Trans. Circuits Syst. II, Exp. Briefs*, vol. 70, no. 4, pp. 1395–1399, Apr. 2023. 

[28] J.-W. Lian, Y.-L. Ban, J.-Q. Zhu, K. Kang, and Z. Nie, “Compact 2-D scanning multibeam array utilizing the SIW three-way couplers at 28 GHz,” *IEEE Antennas Wireless Propag. Lett.*, vol. 17, no. 10, pp. 1915–1919, Oct. 2018. 

[29] C. Wei, Y. Liu, J.-W. Lian, C. Geng, and D. Ding, “Millimeter-wave wide-angle ridge gap waveguide multibeam antenna fed by 3-D printing Butler matrix,” *IEEE Trans. Microw. Theory Techn.*, vol. 73, no. 9, pp. 1–12, Sep. 2025. 

[30] M. Pozar, *Microwave Engineering*, 3rd ed. Hoboken, NJ, USA: Wiley, 2014. 

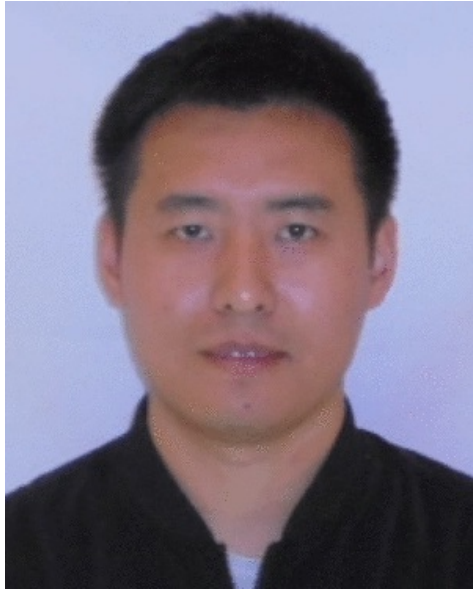
[31] C.-W. Ho, A. E. Ruehli, and P. A. Brennan, “The modified nodal approach to network analysis,” *IEEE Trans. Circuits Syst.*, vol. CS-22, no. 6, pp. 504–509, Jun. 1975. 



[Zhiwei Yin](#) (Graduate Student Member, IEEE) was born in Nantong, Jiangsu, China. He received the B.Sc. and M.S. degrees from Nantong University, Nantong, in 2017 and 2020, respectively. He is currently pursuing the Ph.D. degree at the Faculty of Engineering and Information Technology, University of Technology Sydney (UTS), Sydney, NSW, Australia.

From 2020 to 2023, he worked on Base Station Antenna Research and Development (BSA R&D), COMMScope, Claremont, NC, USA. His current research interests include couplers, phase shifters, power dividers, radio frequency integrated circuits (RFICs), multibeam antennas, and 3-D printing technology.

Mr. Yin won the Best Student Paper Award from the IEEE MTT-S International Microwave Workshop Series on Advanced Materials and Processes for RF and THz Applications (IMWS-AMP) in 2025. He received the HDR Excellence Award from the University of Technology Sydney in 2025.



[He Zhu](#) (Senior Member, IEEE) received [AQ6](#) the bachelor's and master's degrees from South China University of Technology, Guangzhou, China, and the Ph.D. degree in electrical engineering from the School of ITEE, The University of Queensland, Brisbane, QLD, Australia, in 2017. Since July 2017, he has been working with the Global Big Data Technologies Centre (GBDTC), University of Technology Sydney (UTS), Ultimo, NSW, Australia, as a Post-Doctoral Research Associate and then a Chancellor's Research Fellow. In April 2023, he joined the Manufacturing, Commonwealth Scientific and Industrial Research Organisation (CSIRO), Lindfield, NSW, Australia, as an IWY-Research Scientist. His research interests include the development of RF/microwave and terahertz components, integrated circuits and systems, beam-forming antennas and arrays, and superconducting quantum sensors.

Dr. Zhu received the Dean's Award for Outstanding HDR Thesis from the University of Queensland in 2018. He was one of the recipients of the Chancellor's Research Fellowship (CRF) from the University of Technology Sydney in 2022. He was selected as an IWY-Researcher via the Impossible Without You (IWY) Campaign and the Future Science Platform (FSP) from CSIRO in 2023. He received the Rohde & Schwarz Innovation Award from the 2025 IEEE International Workshop on Electromagnetics (iWEM), Hong Kong.



[Xiaojing Lv](#) (Member, IEEE) received the Ph.D. degree in electrical and electronic engineering from The University of Adelaide, Adelaide, SA, South Australia, in 2021.

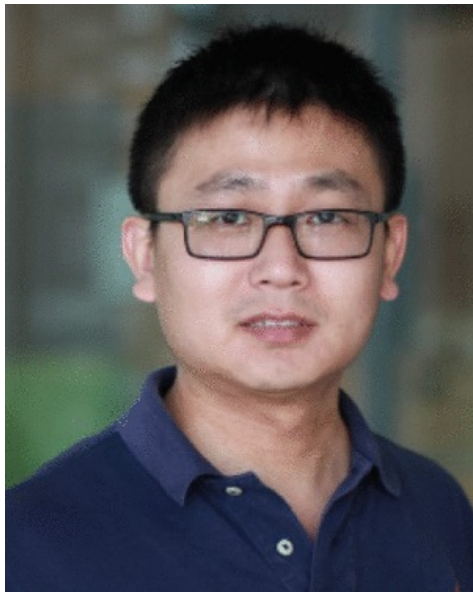
He is currently a Post-Doctoral Research Fellow with the Wireless Communications and Networking Laboratory, TechLab, and a Lecturer at the School of Electrical and Data Engineering, University of Technology Sydney, Sydney, NSW, Australia. His research focuses on computational electromagnetics, advanced metamaterial structures, frequency-selective surface filters, antenna arrays, CubeSat antennas, and multimaterial additive manufacturing.

Dr. Lv was awarded the Australian Government's Research Training Program Scholarship (2017–2021) and won First Place in the Early Career Paper Competition at the International Microwave Symposium (IMS) 2024. He also volunteered in various conference organizing committees, such as Publication Chair of the IEEE MTT-S International Microwave Workshop Series on Advanced Materials and Processes for RF and THz Applications (IMWS-AMP 2026).



[Jiexin Lai](#) (Member, IEEE) was born in Guangdong, China, in 1993. He received the B.S. and M.S. degrees from Shenzhen University, Shenzhen, China, in 2016 and 2020, respectively. He is currently pursuing the Ph.D. degree with the University of Technology Sydney, Ultimo, NSW, Australia.

His research interests include wideband antenna, indoor antenna, metasurface, millimeter-wave, and terahertz wave.









Yang Yang (Senior Member, IEEE) was born in Bayan Nur, Inner Mongolia, China. He received the Ph.D. degree in electronic engineering from the Department of Electrical and Computer Systems Engineering, Monash University, Clayton, VIC, Australia, in 2013.

In 2012, he joined Rain Bird Australia, Melbourne, VIC, Australia, serving as an Asia–Pacific GSP Engineer. In April 2015, he returned to academia, holding the position of Senior Research Associate in microwave and antenna technologies at Macquarie University, Sydney, NSW, Australia. In April 2016, he was appointed as a Research Fellow with the State Key Laboratory of Terahertz and Millimeter Waves, City University of Hong Kong, Hong Kong. In December 2016, he joined the University of Technology Sydney (UTS), Sydney. He is currently a Professor and a Group Leader of 3-D millimeter-wave and terahertz circuits and antennas, UTS TechLab. He has over 300 international publications in microwave, millimeter-wave, and terahertz circuits and antennas. His research interests include additively manufactured electronics, millimeter-wave, subterahertz technologies in 5G and beyond, and biomedical applications.

Dr. Yang is the Australian Research Council Mid-Career Industry Fellow (2025–2029). He is a Committee Member of IEEE AP-S TC-8 Wireless Communication and IEEE MTT-S TC-28 Biological Effects and Medical Applications. From 2022 to 2024, he was a Committee Member of the AP-S Technical Committee on Antenna Measurements and the AP-S Technical Directions Committee. He received many distinguished awards, including the 2025 Advanced Materials Innovation Award by the International Association of Advanced Materials (IAAM), the 2024 IEEE MTT-S IMS First Place in the Early Career Award Competition (serving as the ECR advisor), the 2023 IEEE NSW Section Outstanding Service Award, the 2023 IEEE AP-S Outstanding Chapter Award, and the 2022 IEEE MTT-S Outstanding Chapter Award. His appointments at IEEE NSW Section, Region 10, include the Committee Member of the IEEE NSW Section, the Treasurer (2018–2019) and the Chair/Vice Chair (2020–2024) of the IEEE NSW AP/MTT Joint Chapter, the Secretary (2019) of IEEE NSW PH/ED/SSC/CAS Joint Chapter, and the Inaugural Committee/Treasurer (2020) and Vice Chair (2022–2024) of IEEE NSW Electron Devices Chapter. He also volunteered in various conference organizing committees, such as the General Co-Chair of the 2025 Australian Microwave Symposium, General Co-Chair (Executive Chair) of the Inaugural

Annual International Conference on IEEE Additively Manufactured Electronic Systems (AMES2025), and the General Chair of IEEE MTT-S International Microwave Workshop Series on Advanced Materials and Processes for RF and THz Applications (IMWS-AMP 2026). He serves as the Secretary of the Administrative Committee for the 2026 IEEE MTT-S. He is the Inaugural Chair of IEEE MTT-S TC-17 Microwave Materials and Processing Technologies. He is an Associate Editor of IEEE TRANSACTIONS ON MICROWAVE THEORY AND TECHNIQUES (since October 2022) and IEEE MICROWAVE AND WIRELESS TECHNOLOGY LETTERS (since October 2024), a Guest Editor of PROCEEDINGS OF THE IEEE (2024), an Area Editor of *Microwave and Optical Technology Letters* (2019–2024), an Associate Editor of IEEE ACCESS (2018–2022), and a Guest Editor of IEEE ANTENNAS AND WIRELESS PROPAGATION LETTERS (2022). He was selected as one of the “Top 2% Most Highly Cited Scientists by Stanford” every year since 2019.

Author Query

1. **Query [AQ1]** : Please note that "Multi-Beam" was changed to "Multibeam" in the article title and body text to be in compliance with style guidelines. 
Response by Author: "OK"
2. **Query [AQ2]** : Please confirm or add details for any funding or financial support for the research of this article. 
Response by Author: "Confirmed."
3. **Query [AQ3]** : Please provide the descriptions of part labels (a)–(c) in Fig. 4. 
Response by Author: "(a) Return loss |S11|. (b) Transmission coefficient |S41|. (c) Transmission coefficient |S51|."
4. **Query [AQ4]** : Please provide the appropriate section number for the phrases "following section and aforementioned section" throughout the article. 
Response by Author: "Section III-C"
5. **Query [AQ5]** : Please note that Refs. [2] and [29] were identical in your originally submitted manuscript. Hence, we~have deleted Ref. [29] and renumbered the subsequent references. This will also be reflected in the citations present in the body text. 
Response by Author: "Thank you so much for your help. "
6. **Query [AQ6]** : Please provide the year of completion when the author He Zhu 

received the bachelor's and master's degrees.

Response by Author: "He Zhu received the bachelor's and master's degrees 2011 and 2014, respectively"